Giant spin Hall effect and magnetotransport in a Ta/CoFeB/MgO layered structure: A temperature dependence study

Qiang Hao and Gang Xiao[*]

Department of Physics, Brown University, Providence, Rhode Island 02912, USA
(Received 27 February 2015; revised manuscript received 1 May 2015; published 10 June 2015)

Using an optimized fabrication and magnetic thermal annealing process, we have obtained a high quality β-Ta/CoFeB/MgO layered structure with strong spin-orbit coupling. We have studied electron transport, magnetotransport, and magnetic properties of this system over a wide temperature range between 5 and 300 K. We present the results of resistivity, magnetization, giant spin Hall effect (GSHE), perpendicular magnetic anisotropy, and magnetic switching phase diagram. β-Ta exhibits a large spin Hall angle of 0.14, and shows evidence of spin Hall angle's scaling with resistivity quadratically. The optimized β-Ta/CoFeB/MgO system displays the lowest switching current density among similar systems. Our comprehensive study will benefit applications of GSHE in spintronics.

I. INTRODUCTION

During the last few years, giant spin Hall effect (GSHE) [1–14] has received much attention for its fundamental magnetotransport property and promising potential for spintronics applications, particularly in magnetic random access memories (MRAM), spin logics (SL), rf devices, and magneto-optical components. Solids with large atomic numbers and resistivities, such as Pt [4–8], β-Ta [9], and β-W [10–12], exhibit a very large spin Hall angle (SHA), a key and characterizing parameter of GSHE. The metastable β forms of Ta and W display much larger intrinsic resistivities than their corresponding stable α forms. The origin of GSHE is the enhanced spin-orbit coupling (SOC), based on which the search on solids with even larger SHA continues. Recently it has been shown that some topological insulators are capable of generating phenomenally large GSHE [13,14]. However, transition metals with GSHE have the advantages of compatibility to a semiconductor fabrication process and ability to sustain larger bulk current densities. These transition metals typically carry a SHA in the range of 0.1 to 0.4 [9–12,15–18].

A common method to study the GSHE is to use a bilayer structure consisting of a thin film with large SOC and a ferromagnetic thin film (FM) whose magnetization (**M**) is perpendicular to the bilayer, a property called perpendicular magnetic anisotropy (PMA). A normal longitudinal current in the SOC film induces a large transverse spin current, which exerts a spin-transfer torque (STT) on the **M** of the FM. Above a critical current density (J_C) inside the SOC film, **M** switches its direction abruptly via domain wall motion, which is experimentally measured by using the anomalous Hall effect (AHE) of the FM layer [9,10,12]. To make GSHE useful for MRAM or SL applications, J_C must be reduced as much as possible by virtue of the large SHA and the interfacial match between the SOC and FM layers. A lower J_C reduces power consumption and improves durability in spintronic devices.

In this paper we conducted a comprehensive study on the electron transport, magnetotransport, and magnetic

properties of the β-Ta/CoFeB/MgO system over a wide temperature range (5–300 K). The ferromagnetic thin film CoFeB has the composition of $Co_{40}Fe_{40}B_{20}$. We focused our study on the unique configuration in which the CoFeB displays a robust PMA achieved under an optimal magnetic thermal annealing process. We have obtained the strength of SHA, magnetic anisotropy, and magnetization as functions of temperature. We have also measured the magnetic switching phase diagram, which allowed us to observe the lowest switching current density among similar systems. Our approach shows that a systematic study on multiple properties in these types of systems is highly beneficial to the understanding of the GSHE and its spin-orbit coupling mechanism.

II. EXPERIMENT

We deposited a series of (*t*)Ta/(1)CoFeB/(1.6)MgO (thickness number in nanometer) multilayer stacks on thermally oxidized Si wafers in a homemade high vacuum magnetron sputtering system with a base pressure less than 2×10^{-8} Torr and Ar sputtering pressure ∼2 mTorr. The face-up sputtering guns have a diameter of 5 cm and use an NdFeB permanent magnet ring. The target-substrate distance is 9 cm. The face-down substrates are thermally oxidized single crystal Si wafers (5-cm diameter), which rotate at about 50 rpm during deposition for achieving thickness uniformity. The off-center distance is 3 cm between the center of a substrate and that of a target. A capping layer of (1)Ta was deposited on top of the MgO layer to prevent oxidation of the metal layers from atmosphere. The growth rate of Ta was about 0.5 Å/s under a dc sputtering power of 10 W, and the substrates were kept at ambient temperature. The thin-film stacks were patterned using photolithography into standard Hall bars (20×55 μm^2 in area) for both Hall effect and resistivity measurements. Before measurements, the patterned samples were annealed in vacuum (1×10^{-6} Torr) at different temperatures for 1 h with 2 h of ramping up and 6 h of natural cooling under a magnetic field of 0.45 T perpendicular to the sample planes. We used the Quantum Design®Physical Property Measurement System (PPMS) for magnetization and transport measurement in the temperature range of 5 to 300 K. We also used a
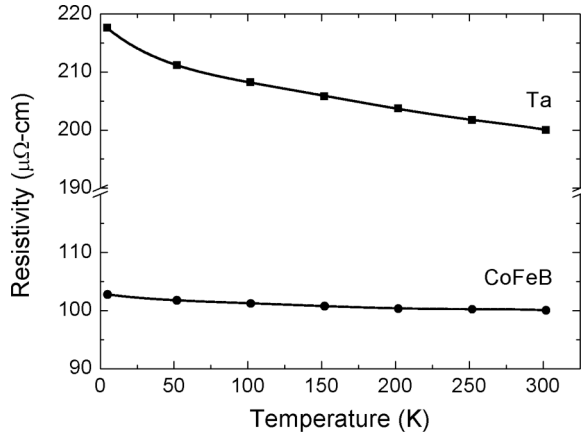
FIG. 1. Resistivities of β-Ta (4 nm thick) and CoFeB (1 nm thick) films as functions of temperature.

few other transport measurement instruments equipped with electromagnets for some measurements.

III. RESULTS AND DISCUSSIONS

To determine the resistivities of Ta and CoFeB films, we measured the sheet resistance (R) of Ta/CoFeB bilayers with different Ta thicknesses ($4 \leqslant t \leqslant 8$ nm). The analysis on the thickness dependent data of R provides the resistivity of the Ta layer ($\rho_{Ta} \approx 200\ \mu\Omega$ cm) and the resistivity of the CoFeB layer ($\rho_{CoFeB} \approx 100\ \mu\Omega$ cm) post-annealing. The high resistivity of Ta is indicative of its β phase, as its α phase has a typical resistivity of $\sim 50\ \mu\Omega$ cm [19,20]. Figure 1 shows the temperature dependence of resistivities for both Ta and CoFeB layers from 5 to 300 K. The resistivity of the CoFeB layer is weakly dependent on temperature (3% variation), ranging from 103 $\mu\Omega$ cm at 5 K to 100 $\mu\Omega$ cm at 300 K. The resistivity of the β-Ta layer also changes little (9% variation) from 218 $\mu\Omega$ cm at 5 K to 200 $\mu\Omega$ cm at 300 K. Therefore, the temperature dependent electron-photon scattering is not the main mechanism for resistivity. Disorder scattering in CoFeB, which is temperature independent, is responsible for its resistivity. The thickness of CoFeB is only 1 nm which sets a limit on the electron mean-free path. The as-prepared CoFeB has an amorphous structure. After post-deposition magnetic annealing, CoFeB retains some of its structural disorder as implied by its high resistivity. The slight increase in the resistivity of the β-Ta layer at low temperatures is interesting. It is not clear what the mechanism is for the resistivity upturn. Low temperature can induce lattice strain on the 4 nm β-Ta thin film and change its band structure somewhat. The resistivity upturn may also be due to some thermally activated electron transport processes. It is noted that the weakly temperature dependent resistivities bode well for spintronics application with regard to thermally stable operation. However, the large resistivity in β-Ta layer does pose a challenge in that the power consumption is somewhat large in order to generate sufficient spin-polarized current using β-Ta.

In our bilayer structures, the CoFeB layer is always fixed at 1 nm which is required for surface-induced PMA. We investigated the magnetic stability of this thin CoFeB layer as a function of temperature. Figure 2(a) shows the in-plane
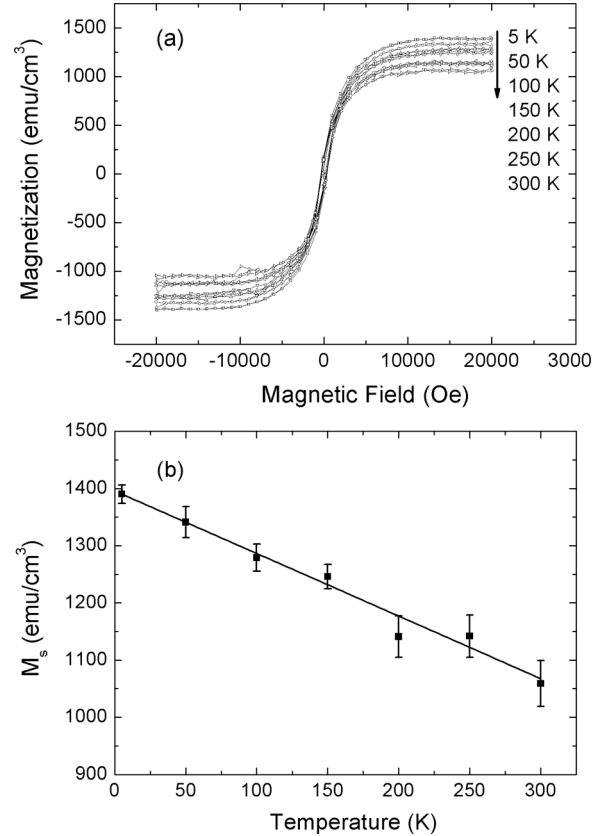

FIG. 2. (a) Magnetization curves of a (4)Ta/(1)CoFeB/(1.6)MgO stack as a function of temperature. The magnetic field is applied in the plane of the stack. (b) Extracted spontaneous magnetization (M_s) as a function of temperature.

magnetization versus magnetic field curves (up to ± 2 T) measured at various temperatures between 5 and 300 K for the (4)Ta/(1)CoFeB/(1.6)MgO sample. A large magnetic field of the order of 0.5 T is required to saturate the magnetization. By extrapolating the magnetization curve within the region of 1 to 2 T to zero field, we extracted the spontaneous magnetization M_s, which is displayed in Fig. 2(b) versus temperature. Within 5 and 300 K, M_s decreases about 23% linearly with temperature, rather than following the Bloch's law of $T^{3/2}$ dependence based on three-dimensional (3D) spin wave excitations. The linear temperature dependence in M_s is due to the 2D nature of our 1-nm-thick CoFeB. It is consistent with observations in other and similar ultrathin ferromagnetic films [21,22]. The measurement of $M_s(T)$ is necessary to study the thermal effect on GSHE to be presented later.

Figure 3 shows the magnetic hysteresis loops (in the format of AHE resistance which is proportional to magnetization) of a series of (4)Ta/(1)CoFeB/(1.6)MgO stacks annealed in vacuum at different temperatures under a perpendicular field of 0.45 T. The as-deposited sample exhibits magnetic in-plane anisotropy. Increasing the annealing temperature cultivates the emergence of a perpendicular magnetic anisotropy (PMA). At 220 °C, a robust PMA is established with a nearly perfect square hysteresis loop. The coercivity H_c is 12 Oe. For our chosen layer structure, 220 °C seems to be the optimized temperature for PMA, as further annealing (270 °C) brings
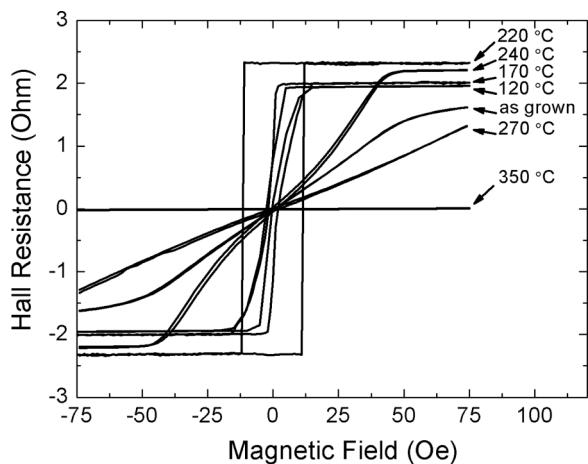
FIG. 3. Anomalous Hall resistance versus magnetic field which is applied perpendicularly to the films, for various (4)Ta/(1)CoFeB/(1.6)MgO stacks annealed at different temperatures.

back the dominance of in-plane magnetic anisotropy again (see Fig. 3). At 350 °C, the AHE disappears due to the possible disintegration of the layered structure. Our results show that the magnetic thermal annealing has a profound influence on the magnetic quality and the PMA of the Ta/CoFeB/MgO system. It seems that a robust PMA is sustained in a well

ordered Ta/CoFeB/MgO structure developed under magnetic annealing at 220 °C. The as-prepared sample has sharp but disordered interfaces, which are unable to support the PMA. On the other hand, higher annealing temperatures (>220 °C) are also deleterious to PMA, most likely due to significant diffusion in the interfacial region. Our finding of the optimal annealing condition is consistent with previous study [23,24]. From here on, we will focus on the (4)Ta/(1)CoFeB/(1.6)MgO stacks annealed at 220 °C.

To measure the SHE in Ta, we measured the magnetotransport of the (4)Ta/(1)CoFeB/(1.6)MgO Hall bar according to the schematic shown in Fig. 4(a). We applied a charge current I along the length of the Hall bar (x axis). As a result, a spin current is generated perpendicular to the Ta layer (along the z axis). An external magnetic field $\boldsymbol{B}_{\text{ext}}$ was applied to the sample within the z-x plane at an angle β to the x axis. The direction of magnetization vector $\boldsymbol{M}$ of the CoFeB layer is controlled by $\boldsymbol{B}_{\text{ext}}$ and the spin-transfer torque (STT) of the SHE-induced spin current. The angle of $\boldsymbol{M}$, defined by the angle θ to the x axis, is determined by measuring the AHE resistance, i.e., $\sin\theta = R_H/R_0$. R_0 is the maximum Hall resistance when $\boldsymbol{M}$ is perpendicular to the sample plane. The equilibrium condition for $\boldsymbol{M}$ is

$$\tau_{\text{tot}} \equiv \hat{x} \cdot (\vec{\tau}_{\text{ST}} + \vec{\tau}_{\text{ext}} + \vec{\tau}_{\text{an}}) = \tau_{\text{ST}}^0 + B_{\text{ext}} \sin(\theta - \beta)$$
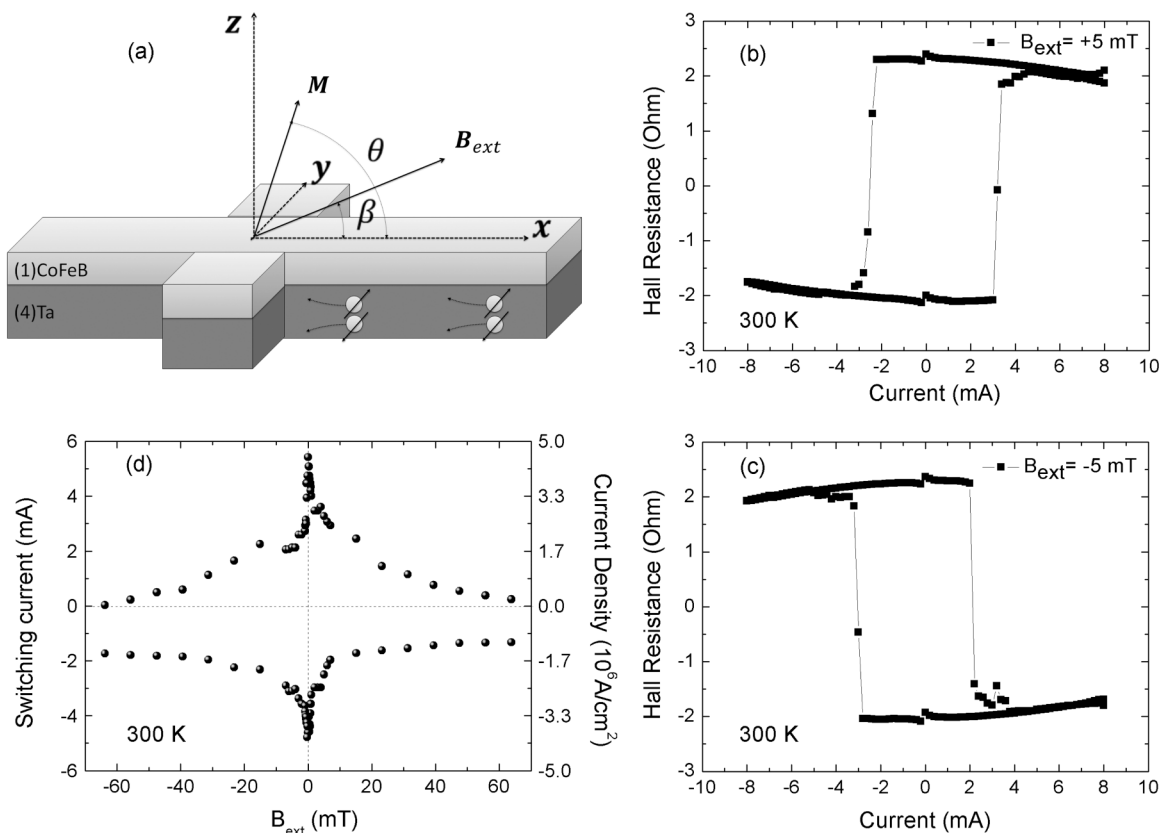$$- B_{\text{an}}^0 \sin\theta \cos\theta = 0 \quad (1)$$

FIG. 4. (a) Schematic drawing of a Ta/CoFeB bilayer in the Hall bar configuration for magnetotransport measurement under an external magnetic field ($\boldsymbol{B}_{\text{ext}}$) and total excitation current ($\boldsymbol{I}$) along the x axis. (b) and (c) Current induced magnetic switching curves in (4)Ta/(1)CoFeB/(1.6)MgO stack under a positive ($\beta = 0°$) and a negative ($\beta = 180°$) external field $\boldsymbol{B}_{\text{ext}}$ of 5 mT. The average total critical current I_C is determined to be 2.7 mA. (d) Magnetic switching phase diagram of a (4)Ta/(1)CoFeB/(1.6)MgO stack in the parameter space of $\boldsymbol{B}_{\text{ext}}$ and total critical current I_C or critical current density J_C (*only* in the Ta layer).
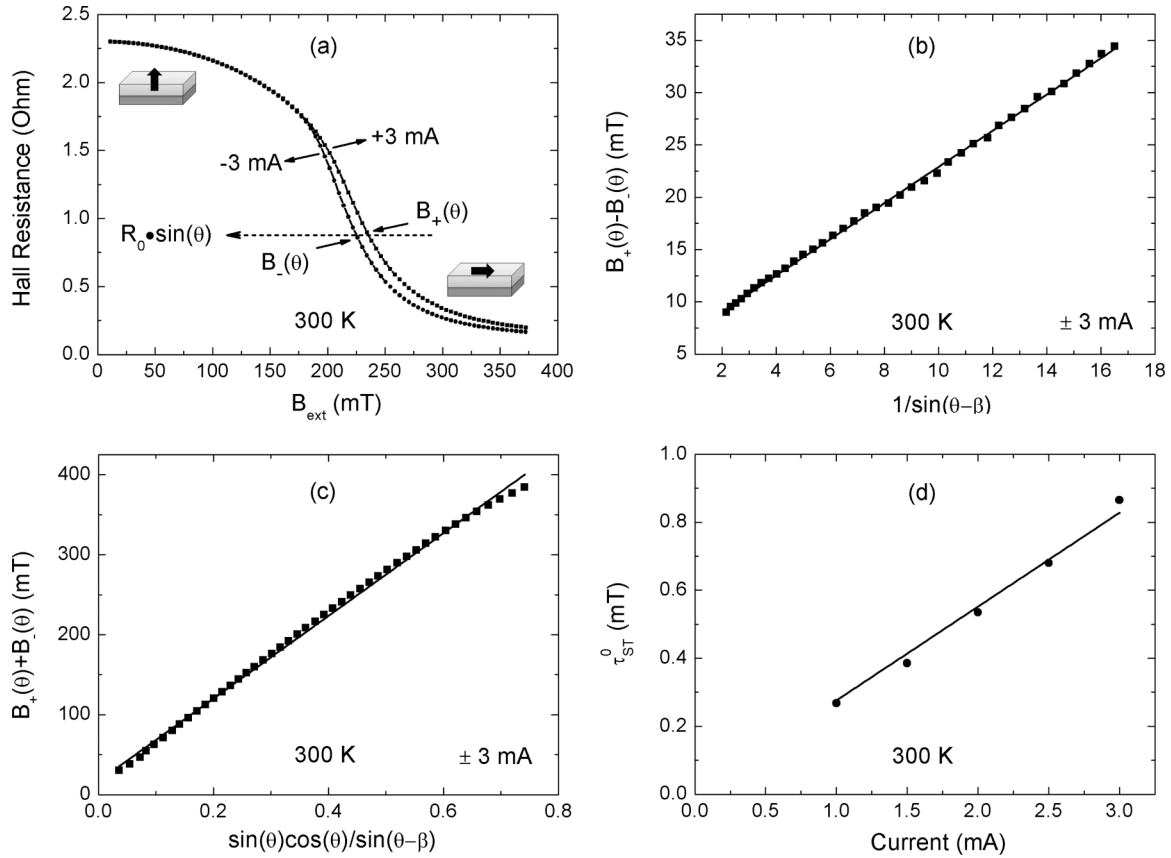
FIG. 5. (a) Anomalous Hall resistance as a function of in-plane magnetic field along the x axis under ± 3 mA excitation currents. θ is the angle between the magnetization vector $\boldsymbol{M}$ and the x axis and can be obtained from the relationship $\sin\theta = R_H/R_0$, where R_0 is the Hall resistance with $\boldsymbol{M}$ is perpendicular to sample plane. (b) Linear relationships between $[B_+(\theta) - B_-(\theta)]$ and $1/\sin(\theta-\beta)$ as expected from Eq. (4). The value of β in our setup is measured to be $2°$. (c) Linear relationships between $[B_+(\theta) + B_-(\theta)]$ and $\sin\theta\cos\theta/\sin(\theta-\beta)$ as expected from Eq. (5). (d) The spin-transfer torque as a function of total excitation current in the Ta/CoFeB/MgO stack. The slope of the linear curve provides the torque per unit of total charge current.

where $\tau_{ST}^0 = \frac{\hbar}{2eM_s t} J_S$, and B_{an}^0 is the perpendicular anisotropy field [25]. According to this macrospin model, a magnetic switching would occur at a critical current density (J_C) which corresponds to a critical STT (τ_{ST}^0). Figures 4(b) and 4(c) show two special cases for such magnetic switching under $B_{ext} = 5$ and -5 mT (along the x axis), respectively. The switching current at approximately 2.7 mA in the bilayer of Ta/CoFeB corresponds to a charge current density in Ta layer of $J_C \approx 2.3 \times 10^6$ A/cm^2. Under a comparable B_{ext}, this observed J_C is the smallest critical current density ever reported in Ta/CoFeB/MgO and Pt/Co/AlO$_x$ systems [9,13,16,25,26].

Figure 4(d) shows our experimentally observed magnetic switching phase diagram of the (4)Ta/(1)CoFeB/(1.6)MgO structure under the influence of B_{ext} (along the x axis) and current (or current density in the Ta layer only). It can be seen that, as we reduce B_{ext}, a larger critical current is required to provide complete switching between M_z and $-M_z$. At $B_{ext} = 0$, consecutive cycling in current leads to partial switching between various magnetic domain states. The switching current density at zero field is determined to be 4.2×10^6 A/cm^2, which is much smaller than previously reported values [13,17,18,27]. To achieve reliable and complete switching, a small field of $B_{ext} = 5$ mT along the x axis is sufficient.

To measure quantitatively the induced STT (τ_{ST}^0) and spin current (J_S) for a given charge current (J_C), we bring our system as shown in Fig. 4(a) into the coherent spin rotation regime, where the $\boldsymbol{M}$ rotates from $90°$ to $0°$ coherently under an increasing B_{ext} along the x axis [see Fig. 5(a)] and a positive or negative charge current. At such moderately high fields (up to 375 mT), we do not need to be concerned with domain wall formation or thermally activated processes. The macrospin model of Eq. (1) is fully valid. Figure 5(a) shows the $R_H (= R_0 \sin\theta)$ of the CoFeB layer as a function of B_{ext} under a positive and a negative current of 3 mA (in Ta/CoFeB bilayer). At an arbitrary $R_0 \sin\theta$, two B_{ext} values exist, $B_+(\theta)$ and $B_-(\theta)$, corresponding to the positive and negative current, respectively. From Eq. (1),

$$\tau_{ST}^0(+J_S) + B_+(\theta)\sin(\theta - \beta) - B_{an}^0 \sin\theta\cos\theta = 0, \quad (2)$$

$$\tau_{ST}^0(-J_S) + B_-(\theta)\sin(\theta - \beta) - B_{an}^0 \sin\theta\cos\theta = 0. \quad (3)$$

By solving the simultaneous equations using the combinations of (2)$\pm$(3), one obtains

$$[B_+(\theta) - B_-(\theta)] = \Delta\tau_{ST}^0/\sin(\theta - \beta), \quad (4)$$

$$[B_+(\theta) + B_-(\theta)] = 2B_{an}^0 \sin\theta\cos\theta/\sin(\theta - \beta), \quad (5)$$

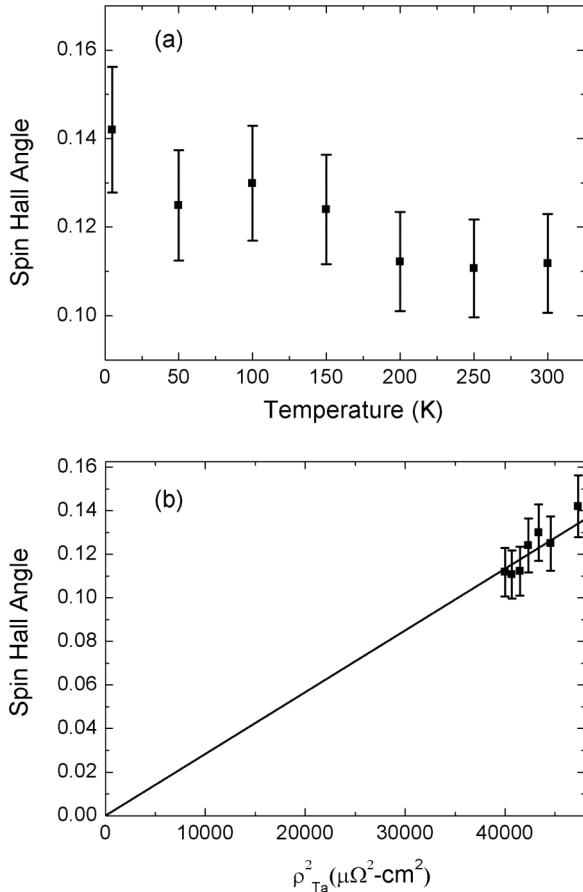FIG. 6. (a) Determined spin Hall angle of β-Ta versus temperature. (b) Scaling relation between spin Hall angle and $\rho_{Ta}{}^2$.

FIG. 7. (a) Square hysteresis loops ($\beta = 90°$) at different temperatures. (b) Coercivity of a (4)Ta/(1)CoFeB/(1.6)MgO stack as a function of temperature.

where $\Delta\tau_{ST}^0 = \tau_{ST}^0(+J_S) - \tau_{ST}^0(-J_S) = 2\tau_{ST}^0(|J_S|)$. The experimental procedure implied in Fig. 5(a) generates the quantities of $B_+(\theta)$, $B_-(\theta)$, and θ. Then, using Eqs. (4) and (5), one can calculate $\tau_{ST}^0(|J_S|)$ and B_{an}^0. Figure 5(b) shows $[B_+(\theta) - B_-(\theta)]$ as a function of $1/\sin(\theta - \beta)$, and Fig. 5(c) shows $[B_+(\theta) + B_-(\theta)]$ as a function of $\sin(\theta)\cos(\theta)/\sin(\theta - \beta)$ based on the data in Fig. 5(a). The value of β in our setup is measured to be $2°$. As predicted by Eqs. (4) and (5), the slopes in Figs. 5(b) and 5(c) are $\Delta\tau_{ST}^0$ and $2B_{an}^0$, respectively. Figure 5(d) shows the STT values $\tau_{ST}^0(|J_S|)$ under various charge currents. As predicted, the STT is proportional to the current. The magnetic anisotropy constant B_{an}^0 remains independent of current. Using the formula for SHA,

$$\Theta = J_S/J_C = \left(\frac{2eM_s t}{\hbar}\right)\left(\tau_{ST}^0/J_C\right) \qquad (6)$$

we calculated the spin Hall angle (Θ) for the 4-nm-thick Ta, which is 0.11 ± 0.01 at 300 K. The main source of Θ uncertainty is in the thicknesses of our films. Also, using Eq. (5), we obtained the magnetic anisotropy constant B_{an}^0, which is 260 ± 5 mT at 300 K.

We have repeated the measurement and analysis over the temperature range of 5–300 K to study the thermal effect on GSHE. Figure 6(a) shows the SHA as a function of temperature. SHA steadily increases (27%) from 0.11 at 300 K to 0.14 at 5 K. In metals with spin-orbit coupling, the anomalous
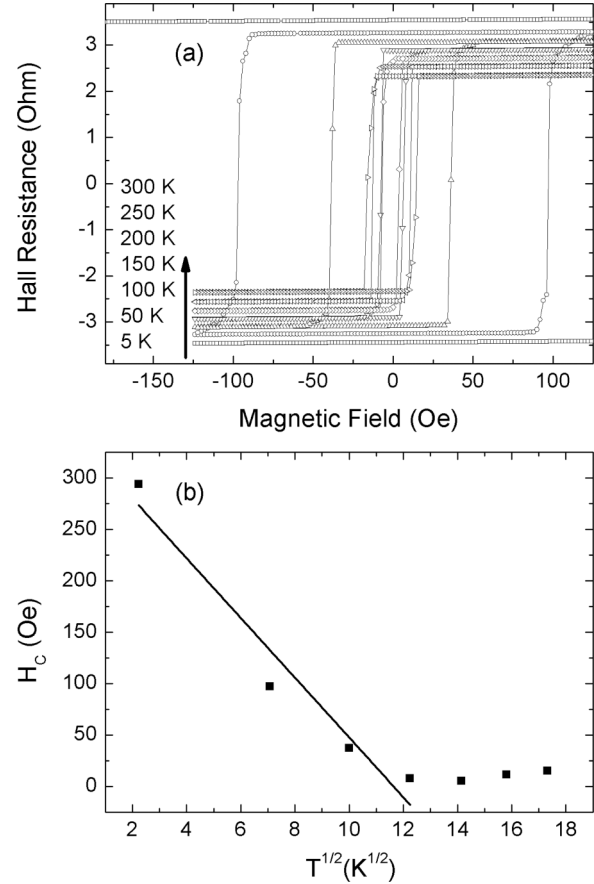
Hall effect scales with resistivity (ρ) linearly or quadratically (ρ^2). The former is due to the extrinsic skew scattering and the latter due to the extrinsic side jump or intrinsic mechanism in spin-orbit coupling [28]. In metals with high resistivity, the scaling relation of Hall angle $\Theta \propto \rho^2$ is most likely. Figure 6(b) shows the spin Hall angle of our samples as a function of ρ^2, which explains our data better than a linear correlation. Due to limited variations in our spin Hall angle and ρ data, more studies are needed to confirm the exact correlation between the spin Hall angle and ρ. However, our observation does indicate a positive correlation between the GSHE and high resistivity.

Next, we focus on the thermal effect of the magnetic properties of the (4)Ta/(1)CoFeB/(1.6)MgO structure, in particular, the coercivity (H_c) and the magnetic anisotropy constant. These are important parameters for applications, because they influence the thermal stability of the magnetic elements such as memory cells. Figure 7(a) shows the hysteresis loops (measured as AHE resistance) between 5 and 300 K in the $\beta = 90°$ configuration. Robust PMA is sustained over the whole temperature range, with squarelike hysteresis loops. Between 150 and 300 K, H_c is low at 10–20 Oe. Below 150 K, H_c increases significantly, reaching 300 Oe at 5 K. The strong temperature dependence in H_c is an indication of the mechanism of thermally activated domain wall (DW)

motion, which predicts the following form:

$$H_c = H_0(1 - aT^{1/2}), \quad (7)$$

where H_0 is the coercivity at 0 K and the constant a depends on the activation energy of DW motion [29–31]. Figure 7(b) shows that between 5 and 150 K, Eq. (7) can account for the temperature dependence of H_c in our sample. Interestingly, between 150 and 300 K, there exists another mechanism for H_c ($\sim$15 Oe) which is nearly independent of temperature. The weakly temperature dependent H_c near room temperature is beneficial to applications.

There are two ways to extract the magnetic anisotropy constant B_{an}^0. The first method is given by Eq. (5), in which a finite charge current is supplied to the Hall bar. In the second method, one can reduce the charge current to nearly zero. Then, Eq. (5) is reduced to

$$B_{ext} = B_{an}^0 \sin(\theta)\cos(\theta)/\sin(\theta - \beta) \quad (8)$$

Figure 4(a) shows the normalized AHE resistance (R_H/R_0), which is $\sin(\theta)$, as a function of an in-plane magnetic field B_{ext}, measured at multiple temperatures between 5 and 300 K. As B_{ext} is varied from -1 T to 0, $\boldsymbol{M}$ rotates coherently from $\theta \sim -180°$ to $-90°$. As B_{ext} increases into the positive field region, above a critical field (H^*), $\boldsymbol{M}$ switches abruptly to $\theta \sim +90°$, and then coherently rotates toward $\theta \sim 180°$ with increasing field strength. The existence of H^* is due to the fact the sample plane is slightly tilted in such a way the in-plane field is not precisely within the plane (i.e., $H_c = H^* \tan\beta$). Based on Fig. 8(a), we plot B_{ext} as a function of $\sin(\theta)\cos(\theta)/\sin(\theta - \beta)$ in Fig. 8(b). As expected from Eq. (8), at every temperature, a complete linear relationship is observed. The slopes of these lines are $B_{an}^0(T)$. Using both methods, we have determined $B_{an}^0(T)$ as shown in Fig. 8(c). The results from the two methods are consistent between each other. $B_{an}^0(T)$ is 0.475 T at 5 K and decreases monotonically to 0.260 T at 300 K.

The large variation of $B_{an}^0(T)$ (73%) within 5 and 300 K is the result of increasing magnetic surface anisotropy constant K_s, which opposes the increasingly large magnetic shape anisotropy (larger M_s) at low temperatures. $B_{an}^0(T)$ consists of two terms, one from magnetic shape anisotropy and the other from PMA, i.e.,

$$B_{an}^0(T) = \frac{2K_s(T)}{tM_s(T)} - 4\pi M_s(T). \quad (9)$$

In Eq. (9), $B_{an}^0(T)$ and $M_s(T)$ have been determined as shown in Figs. 8(c) and 2(b), respectively. The thickness (t) of CoFeB is 1 nm. Therefore, from Eq. (9), we can calculate $K_s(T)$, which is shown in Fig. 9. Over the whole temperature range studied (5–300 K), K_s is linearly dependent on temperature, increasing 85% from 0.84 erg/cm^2 at 300 K to 1.55 erg/cm^2 at 5 K. It is reported in the (2)MgO/(t)CoFeB/(5)Ta/(10)Ru layered structure, the K_s is 1.03 erg/cm^2 at 300 K [32]. The value of K_s is comparable for both systems which share the same interface (MgO/CoFeB) on one side and somewhat different interface on the other side (CoFeB/β-Ta versus CoFeB/Ta/Ru). Therefore, the MgO/CoFeB interface seems to contribute the most to the PMA (K_s). It is a coincidence that both $K_s(T)$ and $M_s(T)$ depend linearly on temperature in our layered structure. We note that $M_s(T)$ is due to the thermally excited spin waves
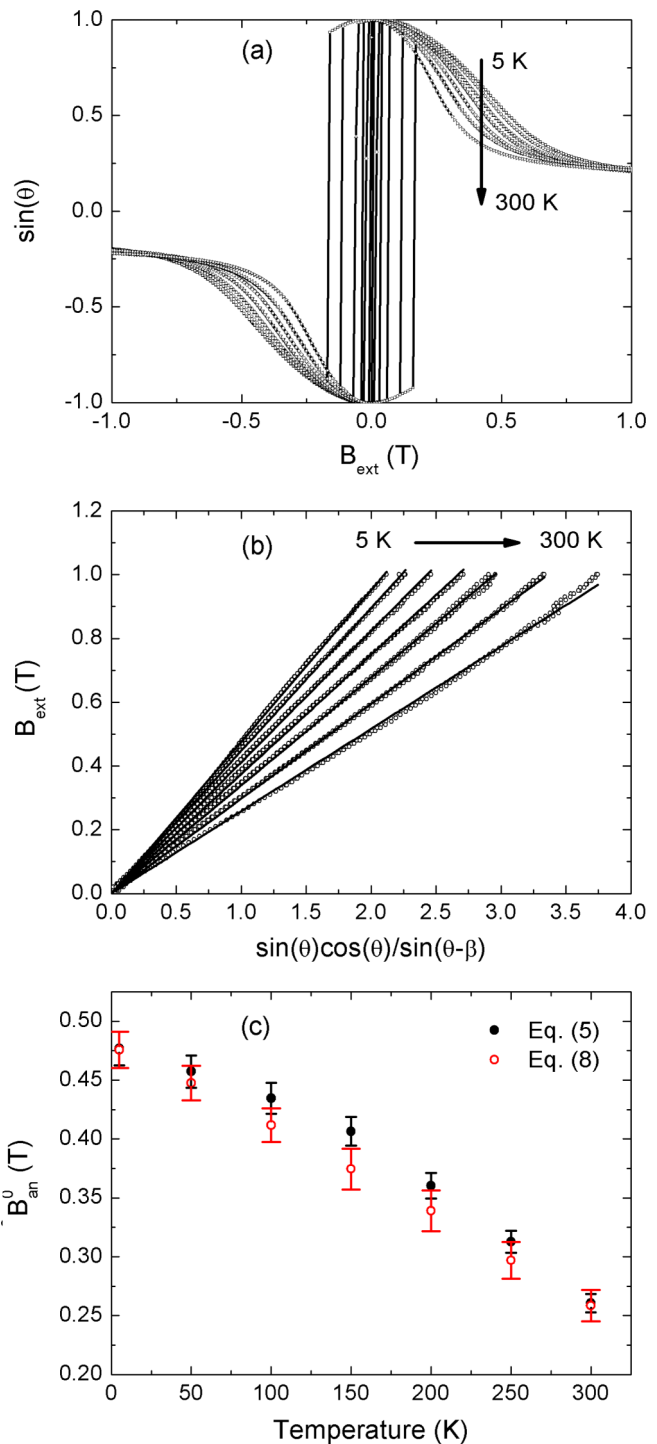

FIG. 8. (Color online) (a) Normalized anomalous Hall resistance ($\sim \sin\theta$) versus nearly in-plane magnetic field ($\beta \sim 0°$) at different temperatures. Switching is caused by the nonzero β angle (slight tilting). (b) The B_{ext} as a linear function of $\sin(\theta)\cos(\theta)/\sin(\theta - \beta)$ with the slope equal to the anisotropy field strength B_{an}^0 according to Eq. (5). (c) The extracted B_{an}^0 as a function of temperature using Eqs. (5) and (6).

in the confinement of a thin film, and is characterized by the exchange coupling and the dimensionality. On the other hand, $K_s(T)$ is characterized by the spin-orbit coupling at the interfaces of a magnetic thin film.
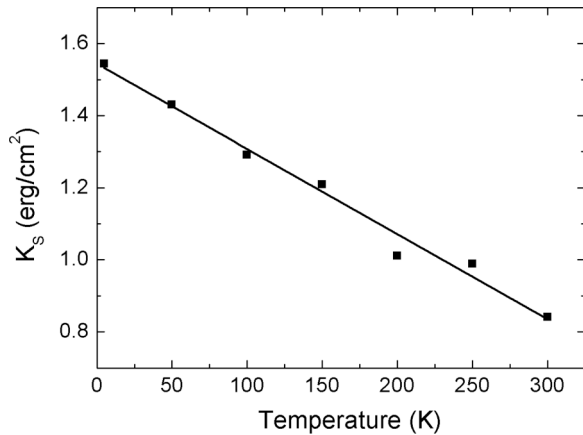
FIG. 9. Perpendicular magnetic surface anisotropy constant (K_s) in a (4)Ta/(1)CoFeB/(1.6)MgO stack as a function of temperature.

IV. CONCLUSIONS

In conclusion, we have performed a comprehensive study on the GSHE and magnetic properties of the (4)Ta/(1)CoFeB/(1.6)MgO spin-orbit coupled system over a wide temperature range between 5 and 300 K. We have optimally annealed the system in high vacuum and in a strong magnetic field, to develop a robust perpendicular

magnetic anisotropy. The spin Hall angle in Ta is very large with a value of 0.14 at 5 K and 0.11 at 300 K. We have determined the magnetic anisotropy field of 0.475 T at 5 K and 0.260 T at 300 K. We have achieved a low switching current density of 2.3×10^6 A/cm^2 in the presence of 5 mT in-plane magnetic field. This is the lowest switching current density among all studies reported on the Ta/CoFeB/MgO systems. The resistivities of the β-Ta and the CoFeB are weakly dependent on temperature, indicating the dominance of electron elastic scatterings from disorder (intrinsic or interfacial) and/or spin-orbit interaction. The spontaneous magnetization of the 1-nm-thick CoFeB layer exhibits linear temperature dependence, rather than following the Bloch's law of spin wave excitations in a 3D system. The GSHA in Ta combining with a ferromagnetic layer with PMA have provided us with a fertile platform to study a plethora of spin dependent transport and magnetic properties. Our results may benefit future spintronic devices such as MRAMs, spin logics, or rf oscillators.

[1] M. I. Dyakonov and V. I. Perel, Phys. Lett. A **35**, 459 (1971).

[2] J. E. Hirsch, Phys. Rev. Lett. **83**, 1834 (1999).

[3] S. Zhang, Phys. Rev. Lett. **85**, 393 (2000).

[4] A. Azevedo, L. H. Vilela-Leão, R. L. Rodríguez-Suárez, A. F. Lacerda Santos, and S. M. Rezende, Phys. Rev. B **83**, 144402 (2011).

[5] N. Vlietstra, J. Shan, V. Castel, J. Ben Youssef, G. E. W. Bauer, and B. J. van Wees, Appl. Phys. Lett. **103**, 032401 (2013).

[6] L. Liu, T. Moriyama, D. C. Ralph, and R. A. Buhrman, Phys. Rev. Lett. **106**, 036601 (2011).

[7] O. J. Lee, L. Q. Liu, C. F. Pai, Y. Li, H. W. Tseng, P. G. Gowtham, J. P. Park, D. C. Ralph, and R. A. Buhrman, Phys. Rev. B **89**, 024418 (2014).

[8] A. Ganguly, K. Kondou, H. Sukegawa, S. Mitani, S. Kasai, Y. Niimi, Y. Otani, and A. Barman, Appl. Phys. Lett. **104**, 072405 (2014).

[9] L. Liu, C.-F. Pai, Y. Li, H. W. Tseng, D. C. Ralph, and R. A. Buhrman, Science **336**, 555 (2012).

[10] C.-F. Pai, M.-H. Nguyen, C. Belvin, L. H. Vilela-Leão, D. C. Ralph, and R. A. Buhrman, Appl. Phys. Lett. **104**, 082407 (2014).

[11] C.-F. Pai, L. Liu, Y. Li, H. W. Tseng, D. C. Ralph, and R. A. Buhrman, Appl. Phys. Lett. **101**, 122404 (2012).

[12] Q. Hao and G. Xiao, Phys. Rev. Appl. **3**, 034009 (2015).

[13] A. R. Mellnik, J. S. Lee, A. Richardella, J. L. Grab, P. J. Mintun, M. H. Fischer, A. Vaezi, A. Manchon, E.-A. Kim, N. Samarth, and D. C. Ralph, Nature (London) **511**, 449 (2014).

[14] Y. Fan, P. Upadhyaya, X. Kou, M. Lang, S. Takei, Z. Wang, J. Tang, L. He, L.-T. Chang, M. Montazeri, G. Yu, W. Jiang, T. Nie,

R. N. Schwartz, Y. Tserkovnyak, and K. L. Wang, Nat. Mater. **13**, 699 (2014).

[15] M. Cubukcu, O. Boulle, M. Drouard, K. Garello, C. O. Avci, I. M. Miron, J. Langer, B. Ocker, P. Gambardella, and G. Gaudin, Appl. Phys. Lett. **104**, 042406 (2014).

[16] X. Qiu, P. Deorani, K. Narayanapillai, K.-S. Lee, K.-J. Lee, H.-W. Lee, and H. Yang, Sci. Rep. **4**, 4491 (2014).

[17] D. Bhowmik, L. You, and S. Salahuddin, Nat. Nanotechnol. **9**, 59 (2014).

[18] S. Emori, E. Martinez, K.-J. Lee, H.-W. Lee, U. Bauer, S.-M. Ahn, P. Agrawal, D. C. Bono, and G. S. D. Beach, Phys. Rev. B **90**, 184427 (2014).

[19] L. A. Clevenger, A. Mutscheller, J. M. E. Harper, C. Cabral, Jr., and K. Barmak, J. Appl. Phys. **72**, 4918 (1992).

[20] M. H. Read and C. Altman, Appl. Phys. Lett. **7**, 51 (1965).

[21] G. Xiao, C. L. Chien, and M. Natan, J. Appl. Phys. **61**, 4314 (1987).

[22] J. Kim, J. Sinha, S. Mitani, M. Hayashi, S. Takahashi, S. Maekawa, M. Yamanouchi, and H. Ohno, Phys. Rev. B **89**, 174424 (2014).

[23] D. C Worledge, G. Hu, D. W Abraham, J. Z. Sun, P. L. Trouilloud, J. Nowak, S. Brown, M. C. Gaidis, E. J. O'Sullivan, and R. P. Robertazzi, Appl. Phys. Lett. **98**, 022501 (2011).

[24] C. O. Avci, K. Garello, C. Nistor, S. Godey, B. Ballesteros, A. Mugarza, A. Barla, M. Valvidares, E. Pellegrin, A. Ghosh, I. M. Miron, O. Boulle, S. Auffret, G. Gaudin, and P. Gambardella, Phys. Rev. B **89**, 214419 (2014).

[25] L. Liu, O. J. Lee, T. J. Gudmundsen, D. C. Ralph, and R. A. Buhrman, Phys. Rev. Lett. **109**, 096602 (2012).

[26] C. Zhang, M. Yamanouchi, H. Sato, S. Fukami, S. Ikeda, F. Matsukura, and H. Ohno, J. Appl. Phys. **115**, 17C714 (2014).

[27] N. Perez, E. Martinez, L. Torres, S.-H. Woo, S. Emori, and G. S. D. Beach, Appl. Phys. Lett. **104**, 092403 (2014).

[28] N. Nagaosa, J. Sinova, S. Onoda, A. H. MacDonald, and N. P. Ong, Rev. Mod. Phys. **82**, 1539 (2010).

[29] Z. Zablotshii, M. Kisielewski, O. Tsiganenko, and J. Ferre, Acta Phys. Polonica A **97**, 471 (2000).

[30] M. Tsai, C. Cheng, C. C. Tsai, and G. Chern, J. Appl. Phys. **113**, 17C118 (2013).

[31] K. Narayanapillai, X. Qiu, J. Rhensius, and H. Yang, J. Phys. D **47**, 105005 (2014).

[32] X. Y. Liu, W. Z. Zhang, M. J. Carter, and G. Xiao, J. Appl. Phys. **110**, 033910 (2011).